Nature of the Charge Density Wave Images of Layered Dichalcogenides 1T-TaX_2 (X = S, Se) in Scanning Tunneling and Atomic Force Microscopy

M.-H. Whangbo,*,† J. Ren,† E. Canadell,*,‡ D. Louder,§ B. A. Parkinson,*,§ H. Bengel,∥ and S. N. Magonov*,∥

Contribution from the Department of Chemistry, North Carolina State University, Raleigh, North Carolina 27695-8204, Laboratoire de Chimie Théorique, Université de Paris-Sud, 91405 Orsay, France, Department of Chemistry, Colorado State University, Fort Collins, Colorado 80523, and Freiburger Materialsforschungszentrum, Albert-Ludwigs Universität, Freiburg D-7800, Germany

Received December 2, 1992

Abstract: Scanning tunneling microscopy (STM) and atomic force microscopy (AFM) images of the charge density wave (CDW) materials 1T-TaX_2 (X = S, Se) were examined by calculating the partial electron density $\rho(r_0, e_f)$ and total electron density $\rho(r_0)$ of a single 1T-$TaSe_2$ layer. Our calculations show that the bright spots of the STM and AFM images are associated with the surface chalcogen atoms, and that both images should possess a pattern of six-chalcogen-atom triangles at CDW maxima. The present study explains why STM images of the CDW's have apparent height amplitudes an order of magnitude greater than the true atomic displacements of the surface chalcogen atoms, why the bright spots of the STM images have a circular shape with a radius smaller than about 2 Å, and why these bright spots appear as three-atom clusters in some images. The patterns of the STM and AFM images predicted from our calculations agree well with those of the observed images.

Introduction

Transition-metal dichalcogenides 1T-MX_2 (M = transition metal, X = S, Se, Te) have layers of composition MX_2, which are constructed from MX_6 octahedra by sharing their edges (Figure 1a).[1] In each MX_2 layer, a sheet of metal atoms is sandwiched between two sheets of chalcogen atoms, and the metal atoms of an undistorted MX_2 layer form a hexagonal lattice (Figure 1b). The 1T-MX_2 compounds with d-electron count d^1 to d^3 exhibit various patterns of metal-atom clustering, which are often referred to as charge density waves (CDW's).[2,3] The 1T-TaX_2 (X = S, Se) systems contain d^1 ions and exhibit a $\sqrt{13} \times \sqrt{13}$ metal-atom clustering (Figure 1c). It has been a topic[3,4] of much discussion whether or not such CDW's originate from the electronic instabilities associated with nesting of their Fermi surfaces (i.e., the solid-state counterpart of the first-order Jahn–Teller instability[5]). In a $\sqrt{13} \times \sqrt{13}$ cluster of 1T-TaX_2 (X = S, Se) (see Figure 2), the Ta(1) and Ta(2) atoms form a centered hexagon (i.e., seven-atom cluster), and the Ta(3) atoms cap the edges of the hexagon. The clustering in the metal-atom sheets induces a periodic lattice distortion in the sandwiching chalcogen-atom sheets. The crystal structure of the $\sqrt{13} \times \sqrt{13}$ CDW state of 1T-$TaSe_2$[6] shows that the Se(1) atoms are farthest away from the metal-atom sheet (at the distance of 1.78 Å), and, with respect to the Se(1) atoms, the Se(2), Se(3), Se(4), and Se(5) atoms are closer to the metal-atom sheet by 0.05, 0.28, 0.26, and 0.25 Å, respectively.

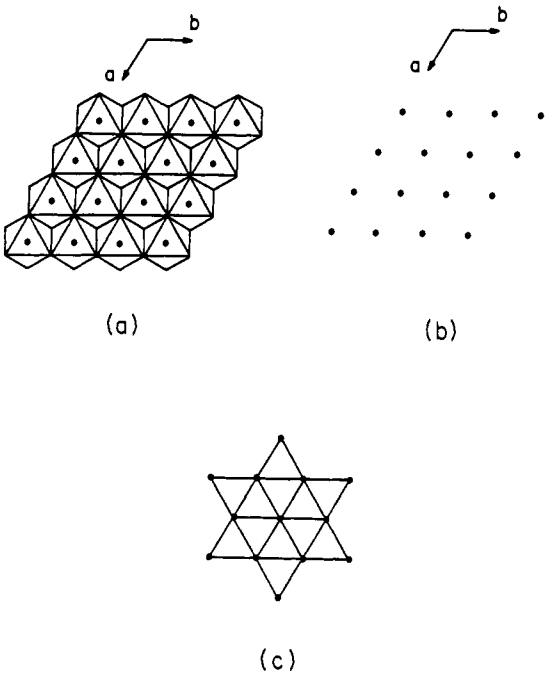

Figure 1. (a) Schematic projection view of an undistorted 1T-MX_2 layer along the c-direction (perpendicular to the layer). (b) Metal ion arrangement in an undistorted 1T-MX_2 layer. (c) $\sqrt{13} \times \sqrt{13}$ clustering of metal atoms in 1T-MX_2 with d^1 ions.

Being held together by van der Waals interactions, individual MX_2 layers of most 1T-MX_2 compounds are easily cleaved to give clean surface so that these compounds are attractive candidates for surface studies with scanning probe techniques such as STM[7,8] and AFM.[9,10] The tunneling current of STM is

† North Carolina State University.
‡ Université de Paris-Sud.
§ Colorado State University.
∥ Albert-Ludwigs Universität.

(1) Hulliger, F. *Structural Chemistry of Layer-Type Phases*; Lévy, F., Ed.; Reidel: Dordrecht, The Netherlands, 1976.
(2) (a) Wilson, J. A.; DiSalvo, F. J.; Mahajan, S. *Adv. Phys.* **1975**, *24*, 117. (b) Williams, P. M. In *Crystallography and Crystal Chemistry of Materials with Layered Structures*; Lévy, F., Ed.; Reidel: Dordrecht, The Netherlands, 1976; Vol. 2, p 51.
(3) (a) *Structure Phase Transitions in Layered Transition Metal Compounds*; Motizuki, K., Ed.; Reidel: Dordrecht, The Netherlands, 1986. (b) Doni, E.; Girlanda, R. In *Electronic Structure and Electronic Transitions in Layered Materials*; Grasso, V., Ed.; Reidel: Dordrecht, The Netherlands, 1986; p 1.
(4) Whangbo, M.-H.; Canadell, E. *J. Am. Chem. Soc.* **1992**, *114*, 9587.
(5) Albright, T. A.; Burdett, J. K.; Whangbo, M.-H. *Orbital Interactions in Chemistry*; Wiley: New York, 1985.
(6) Brouwer, R.; Jellinek, F. *Physica B* **1980**, *99*, 51.
(7) Binnig, G.; Rohrer, H.; Gerber, Ch.; Weibel, E. *Phys. Rev. Lett.* **1982**, *49*, 57.

0002-7863/93/1515-3760$04.00/0

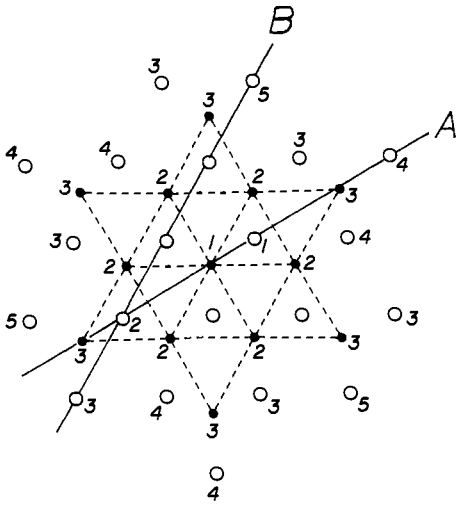

Figure 2. Schematic representation of the three different Ta atoms and five different Se atoms of a $\sqrt{13} \times \sqrt{13}$ cluster in 1T-$TaSe_2$. The Ta and Se atoms are presented by small filled and large empty circles, respectively. The Se atoms of the bottom Se atom sheet are not shown for clarity. The lines *A* and *B* refer to the planes perpendicular to the layer of 1T-$TaSe_2$.

proportional, to a first approximation,[11-13] to $\rho(r_0, e_f)$, the partial electron density of the surface (at the tip-to-surface distance r_0) contributed by the electrons at the energy e_f. For metals e_f is the Fermi level, while for semiconductors e_f usually refers to the highest occupied level in the surface-to-tip tunneling but the lowest unoccupied level in the tip-to-surface tunneling. The $\rho(r_0, e_f)$ plot mimics the STM image in that the higher density region of $\rho(r_0, e_f)$ corresponds to the bright region of the STM image.

The real-space visualization of CDW's in 1T-MX_2 compounds was an exciting event in STM applications, and CDW materials have been extensively studied by STM.[14-16] The STM images of 1T-TaX_2 (X = S, Se) possess an anomalously large amplitude variation (with typical *z* changes in the range of 2–5 Å). The bright spots of the STM images are associated with the $\sqrt{13} \times \sqrt{13}$ clusters, and each spot has a circular shape with a radius smaller than about 2 Å. In some STM images, each bright spot appears as a "three-atom cluster".[15c,16b,17] So far, all these apparently puzzling observations have not been well understood. The Ta-atom sheet of the surface 1T-TaX_2 layer is much farther removed from the STM tip than the surface chalcogen-atom sheet (e.g., 1.78 Å for 1T-$TaSe_2$), so that the Ta contribution to the tunneling current should be negligible compared with the surface chalcogen atom contribution because the amplitude of an atomic orbital decreases exponentially with distance. Indeed, the $\rho(r_0, e_f)$ plots calculated to simulate the STM images of various layered transition-metal compounds [e.g., $ReSe_2$,[18] $NbSe_3$,[19] α-$RuCl_3$,[20] Nb_3X_8 (X = Cl, Br, I),[21] and WTe_2[22]] show that the images are totally dominated by the surface chalcogen or halogen atoms. Therefore, the puzzling aspects of the STM images of the 1T-TaX_2 CDW's should be explained on the basis that the images are dominated by the surface chalcogen atoms.

In a contact AFM, the deflection of the cantilever is mainly caused by the repulsive forces between the tip and the surface, thereby giving rise to the image contrast of the surface. A bright spot of the AFM image is related to a strong repulsive force the tip feels and hence a large charge overlap the tip makes with the surface. Thus, these images can be simulated by the total electron density of the surface $\rho(r_0)$. The detection of CDW's by AFM was unexpected,[23] but it has been achieved with the improvement of instrumentation.[15d,24] The AFM images of 1T-TaX_2 (X = S, Se) possess a much smaller amplitude variation than do the corresponding STM images and were reported[15d] to exhibit the same pattern as observed for the STM images (i.e., a pattern of seven-atom groups at CDW maxima). According to the crystal structure of the CDW of 1T-$TaSe_2$, however, six-chalcogen-atom triangles (formed by the Se(1) and Se(2) atoms) are expected at CDW maxima.

Recently, the STM images[18-21] and AFM images[20,21] of several layered materials were analyzed on the basis of the $\rho(r_0, e_f)$ and $\rho(r_0)$ plots calculated for their layers by employing the extended-Hückel tight-binding (EHTB) electronic band structure method.[25] In the present work, we apply this approach to answer several important questions concerning the STM and AFM images of the CDW's in 1T-TaX_2: Why do the CDW's of 1T-TaX_2 (X = S, Se) exhibit height amplitudes with an order of magnitude greater than the surface chalcogen atoms in STM? Why do the bright spots of the STM images have a circular shape with a radius smaller than about 2 Å? Why do these spots appear as three-atom clusters in some STM images? Why are such spots absent in some STM images?

Experimental Section

Inspection of the reported STM and AFM images of 1T-TaX_2 (X = S, Se) shows that there are definite intensity variations in the atomic-scale patterns representing CDW "hills". To find out the most characteristic images of the CDW's, we have conducted several series of STM and AFM experiments on these compounds. A commercial scanning probe microscope, Nanoscope II, equipped with STM and AFM heads was used in our experiments. Crystals of 1T-TaX_2 (X = S, Se) were glued to conducting supports and cleaved before measurements. Mechanically-sharpened Pt/Ir tips were used for STM, and commercial Si_3N_4 and Si probes for AFM. Atomic-scale images were recorded in the height and current imaging modes for STM, and in the height and force imaging modes for AFM. Some observed images (especially for AFM) were filtered by using the fast Fourier transform (FFT) procedure to emphasize the periodic features of the patterns. In this procedure, the

(8) For recent reviews, see: (a) Hansma, P. K.; Tersoff, J. *J. Appl. Phys.* **1987**, *61*, R1. (b) Tromp, R. M. *J. Phys. Cond. Matter* **1989**, *1*, 10211. (c) Wiesendanger, R., Güntherodt, H.-J., Eds. *Scanning Tunneling Microscopy I, II*: Springer-Verlag: Heidelberg, 1992.

(9) Binnig, G.; Quate, C. F.; Gerber, Ch. *Phys. Rev. Lett.* **1985**, *55*, 394.

(10) Ruger, D.; Hansma, P. *Physics Today* **1990** (October), 23.

(11) (a) Tersoff, J.; Hamman, D. R. *Phys. Rev. B* **1985**, *31*, 805. (b) Tersoff, J. *Phys. Rev. Lett.* **1986**, *57*, 440.

(12) Tersoff, J. In *Scanning Tunneling Microscopy and Related Techniques*; Behm, J., Garcia, N., Rohrer, H., Eds.; Kluwer Academic Publishers: Dordrecht, The Netherlands, 1990; p 77.

(13) (a) Tekman, E.; Ciraci, S. *Phys. Rev. B* **1989**, *40*, 10286. (b) Ciraci, S.; Baratoff, A.; Batra, I. P. *Phys. Rev. B* **1990**, *41*, 2763.

(14) (a) Coleman, R. V.; Drake, B.; Hansma, P. K.; Slough, G. *Phys. Rev. Lett.* **1985**, *55*, 394. (b) Slough, C. G.; McNairy, W. W.; Coleman, R. V.; Drake, B.; Hansma, P. K. *Phys. Rev. B* **1986**, *34*, 994.

(15) (a) Coleman, R. V.; Drake, B.; Giambattista, B.; Johnson, A.; Hansma, P. K.; McNairy, W. W.; Slough, G. *Phys. Scr.* **1988**, *38*, 235. (b) Coleman, R. V.; Giambattista, B.; Hansma, P. K.; McNairy, W. W.; Slough, C. G. *Adv. Phys.* **1988**, *37*, 559. (c) Giambattista, B.; Slough, C. G.; McNairy, W. W.; Coleman, R. V. *Phys. Rev. B* **1990**, *41*, 10082. (d) Coleman, R. V.; McNairy, W. W.; Slough, C. G. *Phys. Rev. B* **1992**, *45*, 1428.

(16) (a) Lieber, C. M.; Xu, X. L. *Acc. Chem. Res.* **1991**, *24*, 170. (b) Wu, X. L.; Lieber, C. M. *Phys. Rev. Lett.* **1990**, *64*, 1150. (c) Wu, X. L.; Lieber, C. M. *Science* **1989**, *243*, 1703.

(17) (a) Wiesendanger, R.; Anselmetti, D. In ref 8c, Vol. I, pp 130–179. (b) Van Bakel, G. P. E. M.; De Hosson, J. Th. M. *Phys. Rev. B* **1992**, *46*, 2001.

(18) Parkinson, B. A.; Ren, J.; Whangbo, M.-H. *J. Am. Chem. Soc.* **1991**, *113*, 7833.

(19) Ren, J.; Whangbo, M.-H. *Phys. Rev. B* **1992**, *46*, 4917.

(20) Ren, J.; Whangbo, M.-H.; Bengel, H.; Magonov, S. N. *J. Phys. Chem.*, in press.

(21) Magonov, S. N.; Zönnchen, P.; Rotter, H.; Cantow, H.-J.; Thiele, G.; Ren, J.; Whangbo, M.-H. *J. Am. Chem. Soc.*, in press.

(22) Tang, S. L.; Kasowski, R. V.; Suna, A.; Parkinson, B. A. *Surf. Sci.* **1991**, *238*, 280.

(23) Heinzelmann, H.; Meyer, E.; Rudin, H.; Güntherodt, H.-J. In *Scanning Tunneling Microscopy and Related Techniques*; Behm, J., Garcia, N., Rohrer, H., Eds.; Kluwer Academic Publishers: Dordrecht, The Netherlands, 1990, p 443.

(24) (a) Barrett, R. C.; Nogami, J.; Quate, C. F. *Appl. Phys. Lett.* **1990**, *57*, 992. (b) Slough, C. G.; McNairy, W. W.; Coleman, R. V.; Garnaes, J.; Prater, B.; Hansma, P. K. *Phys. Rev. B* **1990**, *42*, 9255. (c) Garnaes, J.; Gould, S. A. C.; Hansma, P. K.; Coleman, R. V. *J. Vac. Sci. Technol. B* **1991**, *9*, 1032.

(25) Whangbo, M.-H.; Hoffmann, R. *J. Am. Chem. Soc.* **1978**, *100*, 6093.

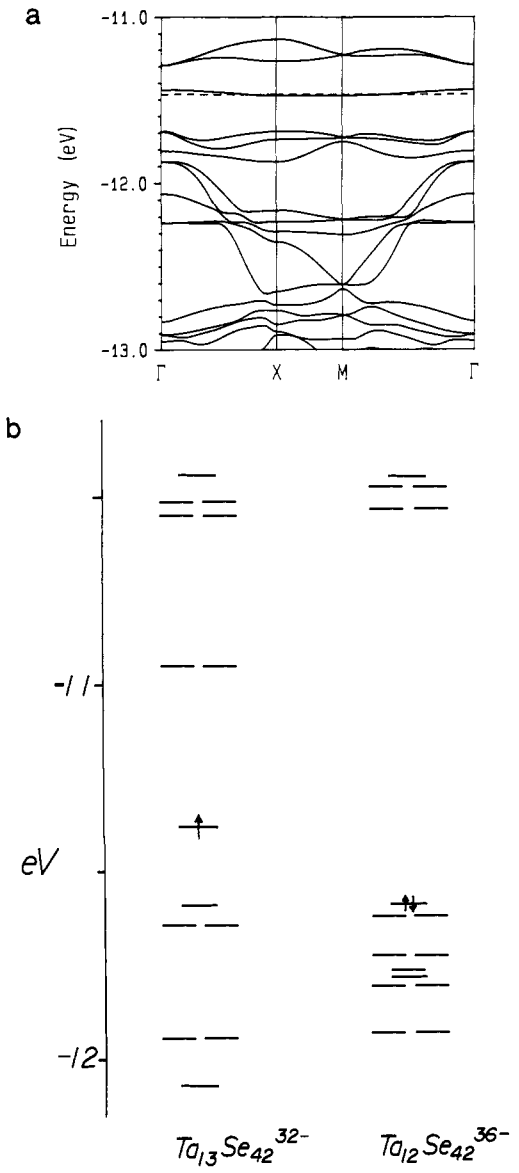

Figure 3. (a) Dispersion relations of the bottom portion of the t_{2g}-block bands calculated for a single 1T-$TaSe_2$ layer with the $\sqrt{13} \times \sqrt{13}$ modulation (see ref 4 for details). The dashed line refers to the Fermi level. (b) Low-lying energy levels of a $\sqrt{13} \times \sqrt{13}$ cluster $Ta_{13}Se_{42}^{32-}$ and the $Ta_{12}Se_{42}^{36-}$ cluster derived from $Ta_{13}Se_{42}^{32-}$ by deleting the Ta(1) atom. For the simplicity of presentation, only the highest occupied levels are shown to have electrons.

pronounced frequency patterns in the FFT power spectra were saved to construct an idealized image in the reverse transform.

Electronic Structure of a Single 1T-$TaSe_2$ Layer

The electronic structure of the $\sqrt{13} \times \sqrt{13}$ CDW state of 1T-$TaSe_2$ was recently examined in some detail.[4] Figure 3a plots the dispersion relations of the bottom portion of the t_{2g}-block bands calculated for a single 1T-$TaSe_2$ layer with the $\sqrt{13} \times \sqrt{13}$ modulation by employing the EHTB method. These bands are mainly derived from the t_{2g}-block levels of each $\sqrt{13} \times \sqrt{13}$ cluster $Ta_{13}Se_{42}^{32-}$ (see Figure 3b). In particular, the highest occupied band is derived from the highest occupied molecular orbital (HOMO) of each $\sqrt{13} \times \sqrt{13}$ cluster. With 13 d electrons per unit cell, the HOMO of each $\sqrt{13} \times \sqrt{13}$ cluster is singly occupied, so that the highest occupied band is half-filled. This band is very narrow (bandwidth of about 0.05 eV[4]) so that the electrons of the highest-occupied band are

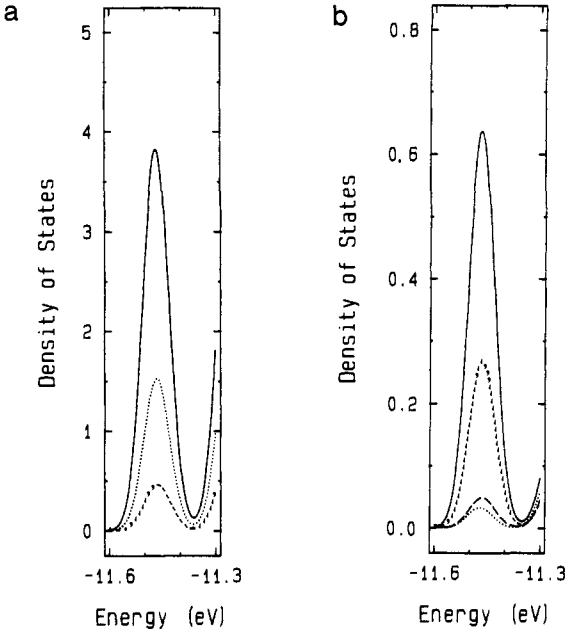

Figure 4. (a) PDOS values per atom calculated for the Ta(1) (solid line), Ta(2) (dotted line), and Ta(3) (dashed line) atoms of 1T-$TaSe_2$. (b) PDOS values per atom calculated for the Se(1) (solid line), Se(2) (short-dash line), Se(4) (long-dash line), and Se(5) (dotted line) atoms of 1T-$TaSe_2$. The PDOS values per atom for the Se(3) are practically identical with those for the Se(5) atom, and hence are not shown.

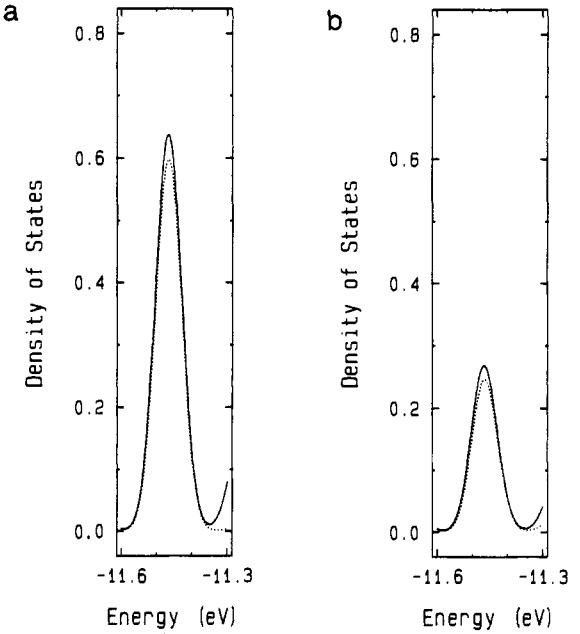

Figure 5. (a) PDOS values per atom of the Se(1) atom (solid line) and its $4p_z$ orbital contribution (dotted line). (b) PDOS values per atom of the Se(2) atom (solid line) and its $4p_z$ orbital contribution (dotted line).

susceptible to localization, as indeed found for 1T-TaS_2.[26] The highest-occupied band is largely responsible for the $\rho(r_0, e_f)$ plot and hence the STM image. Thus, it is important to analyze the orbital compositions of this band in some detail. Figure 4 shows the projected density of states (PDOS) calculated for the three different Ta and five different Se atoms of 1T-$TaSe_2$. Figure 5 compares the PDOS plots of the Se(1) and Se(2) atoms (solid line) with their $4p_z$ orbital contributions (dotted line). (The coordinate z-axis is perpendicular to the 1T-$TaSe_2$ layer, and so the Se $4p_z$ orbitals are perpendicular to the layer.) Important

(26) Dardel, B.; Grioni, M.; Malterre, D.; Weibel, P.; Baer, Y.; Lévy, F. *Phys. Rev. B* **1992**, *45*, 1462.

observations to note from Figures 4 and 5 are as follows. (a) The highest-occupied band has a greater contribution from the Ta atoms than from the Se atoms. (b) The Ta contribution (per atom) to the highest-occupied band decreases in the order, Ta(1) > Ta(2) > Ta(3). (c) The Se contribution (per atom) to the highest-occupied band decreases in the order, Se(1) > Se(2) ≫ Se(4), Se(3), Se(5). (d) The contributions of the Se(1) and Se(2) atoms to the highest-occupied band are given almost exclusively by their $4p_z$ orbitals.

The crystal structure of the $\sqrt{13} \times \sqrt{13}$ CDW state of 1T-TaS_2 is not available. However, since 1T-TaS_2 and 1T-$TaSe_2$ possess similar structures and physical properties, it is expected that conclusions (a)–(d) are also applicable to 1T-TaS_2.

Electron Density Plots

The individual layers of most layered transition-metal compounds are held by van der Waals interactions, and thus the structures of the surface layers should be practically identical with those of the layers in the bulk. Therefore, we calculate the $\rho(r_0)$ and $\rho(r_0, e_f)$ plots of a single 1T-$TaSe_2$ layer on the basis of its electronic structure obtained from the EHTB method. In our calculations of $\rho(r_0)$ and $\rho(r_0, e_f)$, the r_0 value was taken to be 0.5 Å (i.e., 0.5 Å away from the atoms closest to the tip). The orbital amplitudes of the wave functions of a surface decrease exponentially with distance from the surface, so that the $\rho(r_0, e_f)$ values become too small for meaningful comparisons if r_0 is chosen to be much larger than 0.5 Å (e.g., $r_0 = 4$ Å). The values calculated for $r_0 = 0.5$ Å have been found to accurately reflect the tunneling probabilities from a more distant tip for many layered materials.[18-22] Furthermore, in a simultaneous STM/AFM study of 1T-TaS_2 at ambient conditions,[24a] the STM image obtained with the tip in contact with the surface is nearly identical with that registered in a traditional STM study. Consequently, the $\rho(r_0, e_f)$ plot calculated for a small r_0 value can be used for the interpretation of the STM images.

Figure 6 shows that the $\rho(r_0)$ plot of a single 1T-$TaSe_2$ layer has density distributions exclusively on the surface Se atoms. In each unit cell of the $\rho(r_0)$ plot, the electron density of the Se atom decreases in the order, Se(1) ≥ Se(2) > Se(3), Se(4), Se(5). This is consistent with the finding that the distances of the surface Se atoms to the tip increase in the order, Se(1) > Se(2) ≫ Se(3), Se(4), Se(5). Consequently, the $\rho(r_0)$ plots of Figure 6 predict that the bright spots of the AFM image are caused by the surface Se atoms, and that the AFM images should exhibit a pattern of six-chalcogen-atom triangles at CDW maxima. Such a pattern is found in the reported AFM images of 1T-$TaSe_2$.[24b]

The $\rho(r_0, e_f)$ plots of a single 1T-$TaSe_2$ layer, shown in Figure 7, were obtained by sampling all levels of the highest-occupied band of Figure 3. The $\rho(r_0, e_f)$ plots calculated by sampling only those energy levels lying within a very small energy window from the Fermi level are essentially the same as those shown in Figure 7 because the orbital compositions of the highest-occupied band are nearly uniform throughout the band (see Figure 4). The $\rho(r_0, e_f)$ plots of Figure 7 show that electron density distribution has no contribution from the Ta atoms, and arises exclusively from the surface Se(1) and Se(2) atoms. Practically, there is no contribution from the Se(5) atoms, and the electron density decreases in the order, Se(1) > Se(2) ≫ Se(3), Se(4). This is consistent with observation (c) and also with the fact that the Ta atoms are much farther away from the tip than the surface Se atoms. The peaks of the $\rho(r_0, e_f)$ plot for the Se(1) and Se(2) atoms (Figure 7) are centered at the atomic positions, which arises from observation (d).

Figure 8 shows the cross-sectional view of the partial electron density of a single 1T-$TaSe_2$ layer (associated with the band levels at the Fermi level) in the plane *A* perpendicular to the layer (defined in Figure 2). This cross section contains the Se(1), Se(2), Se(4), and Ta(1) atoms of a $\sqrt{13} \times \sqrt{13}$ cluster. The

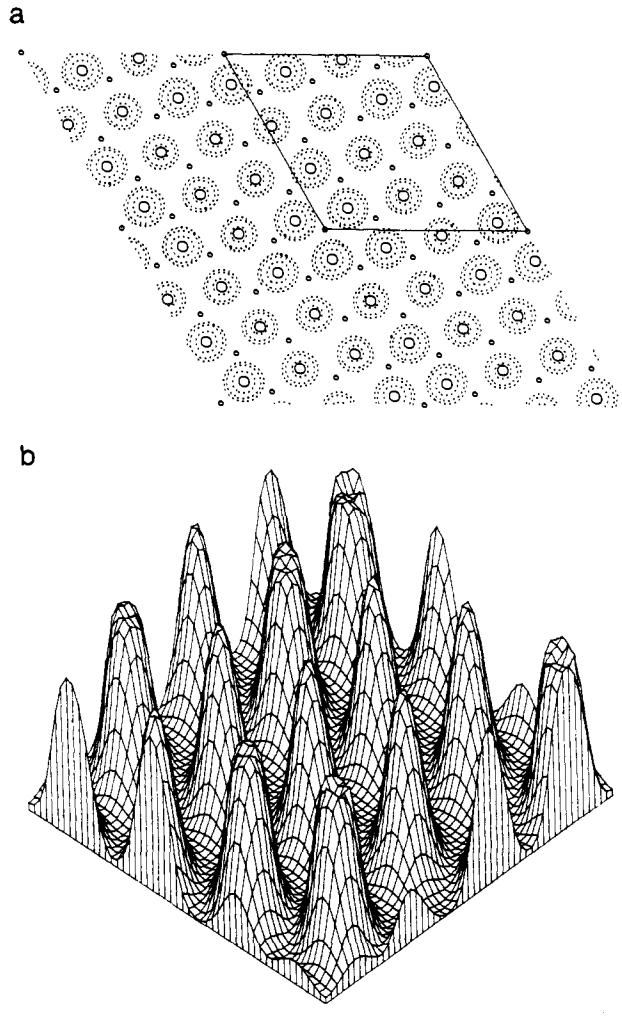

Figure 6. $\rho(r_0)$ plots calculated for a single layer of 1T-$TaSe_2$. (a) Two-dimensional contour representation. The plot area consists of four unit cells, and a unit cell is indicated by a rhombus. The contour values used are 10, 5, and 3×10^{-2} e/au^3. For clarity, the Se atoms on the bottom surface are not shown. The Ta and Se atoms are shown by small and large circles, respectively. (b) Three-dimensional surface representation. The plot area consists of one unit cell.

Ta atom density is strong largely inside the sandwiching Se-atom sheets and practically negligible outside the Se-atom sheets. Therefore, it is clear from Figures 7 and 8 that the bright spots of the STM image are caused mainly by the surface Se(1) and Se(2) atoms, and that the STM image should exhibit a pattern of six-chalcogen-atom triangles at CDW maxima, with the inner triangle of the Se(1) atoms much brighter than the outer triangle of the Se(2) atoms. Thus, the bright spots of the STM images, of the size of a circle with radius of about 2 Å or less, should be associated with the inner triangles of the Se(1) atoms of the $\sqrt{13} \times \sqrt{13}$ clusters. These bright spots should appear as three-atom clusters in STM images of atomic resolution, which provides a natural explanation for the observation of such patterns in some cases.[15c,16b,17]

Our calculations show that the corrugations in the $\rho(r_0, e_f)$ plot are much greater than that in the $\rho(r_0)$ plot (compare Figures 6 and 7), which is consistent with the finding that the amplitude of the CDW modulation in the STM image is much stronger than that in the AFM image. To explain the anomalously large amplitude of the CDW modulation, we show in Figure 9 the cross-sectional view of the partial electron density of a single 1T-$TaSe_2$ layer (resulting from the band levels at the Fermi level) in the plane *B* perpendicular to the layer (Figure 2). This cross section contains the Se(1), Se(2), Se(3), and Se(5) atoms of a $\sqrt{13} \times \sqrt{13}$ cluster. It is evident from Figures 7 and 9 that the

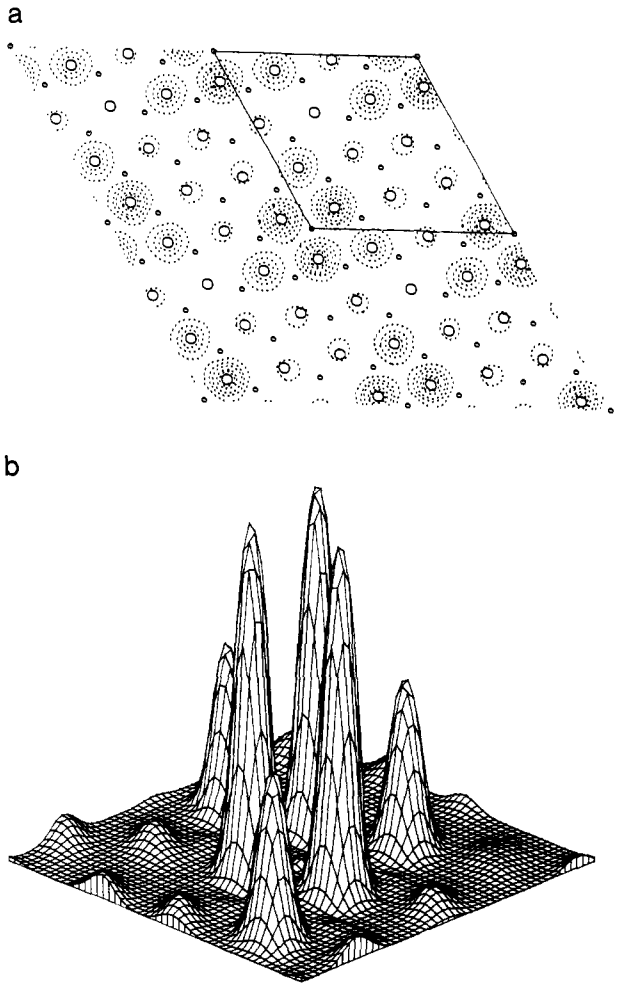

Figure 7. $\rho(r_0, e_f)$ plots calculated for a single layer of 1T-$TaSe_2$: (a) Two-dimensional contour representation. The plot area consists of four unit cells, and a unit cell is indicated by a rhombus. The contour values used are 25, 20, 10, 5, and 1×10^{-4} e/au^3. For clarity, the Se atoms on the bottom surface are not shown. The Ta and Se atoms are shown by small and large circles, respectively. (b) Three-dimensional surface representation. The plot area consists of one unit cell.

$\rho(r_0, e_f)$ plots are dominated by the $4p_z$ orbitals of the surface Se(1) and Se(2) atoms. The STM height image is simulated by the contour plot of constant electron density in Figure 9 (and Figure 8 as well). Compared with the Se(1) and Se(2) positions, the electron density at the Se(3), Se(4), and Se(5) positions are very small. Figure 9 clearly shows that the z-height difference in the contour lines can easily reach 2 Å, which is consistent with the anomalously large amplitude of the CDW experimentally observed.

The above analysis shows that the STM image of 1T-$TaSe_2$ is primarily governed by the partial electron density associated with the highest occupied band of the surface $TaSe_2$ layer. As already mentioned, this band is largely made up of the HOMO from each $\sqrt{13} \times \sqrt{13}$ cluster. In other words, each bright spot of the STM image represents the electron density given by the HOMO of the corresponding $\sqrt{13} \times \sqrt{13}$ cluster. The tunneling current is sensitive only to the partial electron density associated with the Fermi level. Thus, if the HOMO level of a $\sqrt{13} \times \sqrt{13}$ cluster is made lower than that of other $\sqrt{13} \times \sqrt{13}$ cluster units, then such a cluster cannot contribute to a tunneling current and hence should appear as dark in the STM image as if the whole cluster is absent. This kind of situation is likely to occur when the Ta(1) atom of a $\sqrt{13} \times \sqrt{13}$ cluster is absent as illustrated in Figure 3b, which compares the calculated

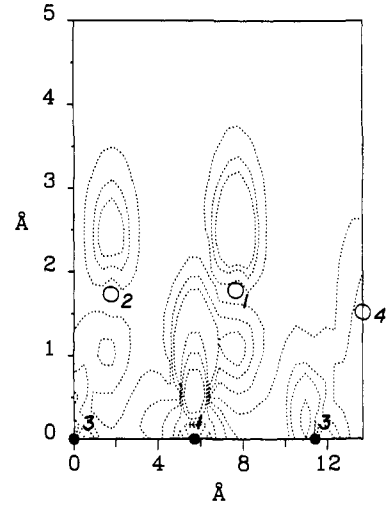

Figure 8. Cross-sectional view of the partial electron density distribution of a single 1T-$TaSe_2$ layer (resulting from the band levels at the Fermi level) in the plane A, perpendicular to the layer, defined in Figure 2. The Ta and Se atoms are represented by small filled and large empty circles, respectively. This cross section contains the Se(1), Se(2), Se(4), Ta(1), and Ta(3) atoms of a $\sqrt{13} \times \sqrt{13}$ cluster. The contour values used are 200, 100, 50, 10, 5, and 1×10^{-2} e/au^3.

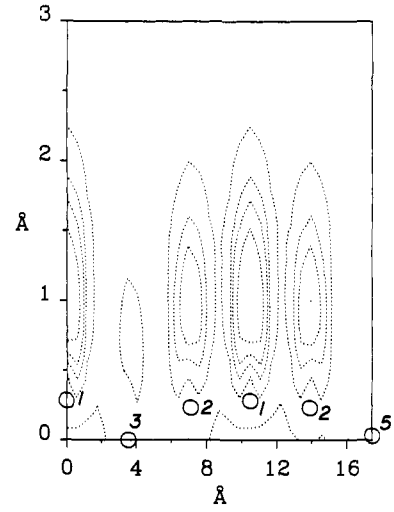

Figure 9. Cross-sectional view of the partial electron density distribution of a single 1T-$TaSe_2$ layer (resulting from the band levels at the Fermi level) in the plane B, perpendicular to the layer, defined in Figure 2. The Se atoms are represented by empty circles. This cross section contains the Se(1), Se(2), Se(3), and Se(5) atoms of a $\sqrt{13} \times \sqrt{13}$ cluster. The contour values used are 20, 10, 5, and 1×10^{-4} e/au^3.

energy levels of a $\sqrt{13} \times \sqrt{13}$ cluster $Ta_{13}Se_{42}^{32-}$ with those of the $Ta_{12}Se_{42}^{36-}$ cluster derived from it by deleting the Ta(1) atom.

STM and AFM Images of 1T-TaX_2 (X = S, Se)

On the basis of the theoretical results discussed above, we now examine the experimental STM and AFM images of 1T-TaX_2 (X = S, Se). Numerous variations occur in the details of the images, so that it is difficult to select the most characteristic atomic-scale images. Of several reasons for the image variations, the asymmetry of the tip apex is the most crucial one. According to the crystal structure and the electron density distribution of 1T-TaX_2 (X = S, Se), there is no compelling reason for the distortion of the STM and AFM images. Consequently, the atomic-scale images with highly symmetric patterns can be chosen as the most characteristic. The STM image of 1T-TaS_2 presented in Figure 10 meets this requirement, where the atomic and the CDW corrugations are clearly seen. One of the frequently

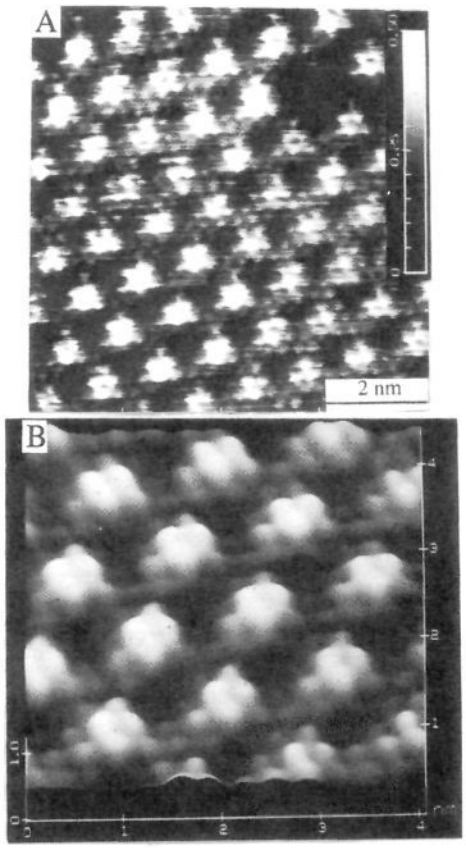

Figure 10. STM current images of 1T-TaS_2 obtained with the set-point tunneling current I_{tun} = 6 nA and the bias voltage V_{bias} = −10 mV. The vertical gray-scale bar indicates the image corrugations proportional to the logarithm of the tunneling current I, i.e., $\ln(I)$, in the direction perpendicular to the examined surface: (A) unfiltered image, (B) filtered image (a zoomed part of A) shown as a surface plot.

observed defects is also present at the upper right hand corner of the image in Figure 10a, which appears as if one whole CDW "hill" is missing. As already pointed out, a Ta(1) atom vacancy in a $\sqrt{13} \times \sqrt{13}$ cluster can cause such a defect. A pronounced triangular pattern is clearly seen in the center of each CDW "hill" (Figure 10b). This pattern is registered as one spot with radius smaller than about 2 Å, if an atomic resolution is not achieved. The $\rho(r_0, e_f)$ plot of Figure 8 agrees well with the STM images of 1T-TaS_2 shown in Figure 10 and reported already in the literature.[15c,16b,24a] Similar patterns with pronounced three-atom clusters are also found in the reported STM images of 1T-$TaSe_2$.[15c,17]

In general, the quality of the AFM images is inferior to that of the STM images. Thus, we perform the FFT filtration to reveal fine details of the AFM image although this makes it difficult to find the experimental image with high symmetry. The AFM image of 1T-TaS_2 presented in Figure 11 is very similar to that first reported[24a] and clearly shows the atomic and CDW corrugations. The number of protrusions in the AFM images in general agrees with that expected from the $\rho(r_0)$ plot. The atomic protrusions of each CDW "hill" have a much more uniform intensity distribution in AFM than in STM. As a result, it is difficult to determine a reliable intensity distribution in the AFM image.

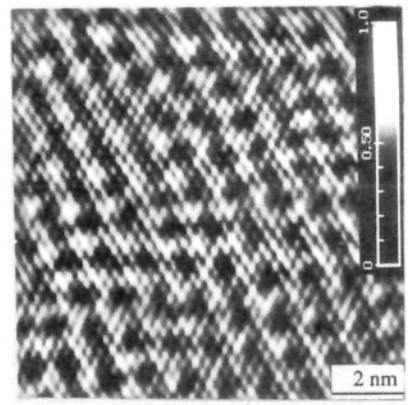

Figure 11. AFM force image of 1T-TaS_2. The vertical gray-scale bar indicates the force corrugations in nN in the direction perpendicular to the examined surface.

The STM and AFM images of 1T-$TaSe_2$ are very similar to those of 1T-TaS_2 (and hence not shown). Thus, the STM and AFM images of the CDW's in 1T-TaX_2 (X = S, Se) are well explained by the $\rho(r_0, e_f)$ and $\rho(r_0)$ plots calculated for the CDW state of 1T-$TaSe_2$. The present work provides a strong support for the use of the $\rho(r_0, e_f)$ and $\rho(r_0)$ plots in the interpretation of STM and AFM images.

Concluding Remarks

Our study reveals that the bright spots of both the STM and AFM images of 1T-TaX_2 (X = S, Se) are associated with the surface chalcogen atoms. The STM images should possess a pattern of six-chalcogen-atom triangles of the Se(1) and Se(2) atoms at CDW maxima, with greater contribution from Se(1). This explains the typical size of the bright spots of the STM images and their splitting into a three-atom cluster in certain cases. Certainly, the CDW modulations of 1T-TaX_2 (X = S, Se) are induced by the d electrons of Ta,[4] and their highest occupied bands are dominated by the Ta atoms. Nevertheless, it is the surface chalcogen atoms, the minor component of the highest occupied bands, that determine the STM pattern because of their proximity to the scanning tip. The Ta atoms are too far away from the scanning tip to contribute to the tunneling current. Like the STM images, the AFM images should possess a pattern of six-chalcogen-atom triangles of the S(1) and Se(2) atoms at the CDW maxima.

The large difference in the height amplitudes of the STM and AFM images simply reflects the difference in the density distributions of the $\rho(r_0)$ and $\rho(r_0, e_f)$ plots. Observations (c) and (d), together with the fact that the surface Se(1) and Se(2) atoms are closer to the scanning tip than any other atoms by about 0.25 Å, explain why the amplitude of the CDW modulation is so large in the STM image. The small amplitude of the CDW modulation in the AFM image is not surprising because the $\rho(r_0)$ plot mimics the surface topography and because the amplitude of the height modulation in the surface chalcogen atoms is of the order of 0.3 Å.

Acknowledgment. Work at North Carolina State University was supported by the Office of Basic Energy Sciences, Division of Materials Sciences, U.S. Department of Energy, under Grant DE-FG05-86ER45259, and by Scientific Affairs Division, NATO, under Grant CRG 910129.